Silicon Photomultiplier Technology at STMicroelectronics

Massimo Mazzillo, Giovanni Condorelli, Delfo Sanfilippo, Giuseppina Valvo, Beatrice Carbone, Giorgio Fallica, Sergio Billotta, Massimiliano Belluso, Giovanni Bonanno, Luigi Cosentino, Alfio Pappalardo, and Paolo Finocchiaro

***Abstract*—In this paper we present the results of the first electrical and optical characterization performed on 1 mm^2 total area Silicon Photomultipliers (SiPM) fabricated in standard silicon planar technology at the STMicroelectronics Catania R&D clean room facility. The device consists of 289 microcells and has a geometrical fill factor of 48%. Breakdown voltage, gain, dark noise rate, crosstalk, photon detection efficiency and linearity have been measured in our laboratories. The optical characterization has been performed by varying the temperature applied to the device. The results shown in the manuscript demonstrate that the device already exhibits relevant features in terms of low dark noise rate and inter-pixel crosstalk probability, high photon detection efficiency, good linearity and single photoelectron resolution. These characteristics can be considered really promising in view of the final application of the photodetector in the Positron Emission Tomography (PET).**

***Index Terms*—Crosstalk, dark noise rate, gain, Geiger mode avalanche photodiode, linearity, photon detection efficiency, silicon photomultiplier.**

I. Introduction

SILICON PHOTOMULTIPLIERS (SiPM) have known a fast development in the last few years as a possible alternative to vacuum photomultiplier tubes (PMT) and avalanche photodiodes (APD). Originally developed in Russia in the mid-1980s [1], SiPM detectors are currently produced by different manufacturers and the technology is now maturing [2]–[8].

As compared to PMT and APD, SiPM have numerous advantages such as low bias voltage operation ($<$100 V), high Photon Detection Efficiency (PDE) for visible and near infrared photons, excellent single-photon response, fast rise time ($\ll$1 ns), low power consumption, insensitivity to magnetic fields, compactness, and mechanical robustness. Moreover the SiPM has a gain (10^5 to 10^6) comparable to a PMT but much higher than in an APD (10^2 to 10^3).

Finally the solid-state detector approach has the typical advantages of the planar process integration; therefore SiPM can be manufactured at low cost and reproducibly.

The main drawback currently limiting the SiPM performance is the high dark noise rate, which primarily originates from the carriers thermally generated in the sensitive volume. This parameter can limit the detector signal to noise ratio, especially at high temperature and for large sensitive area and needs to be reduced by improving the device manufacturing technology. However, SiPM's dark noise rate limits the detector performance only in detection of very weak photon intensities (one or a few photoelectrons) and it does not affect in the case of higher light signals.

In previous papers we described the design and characterization of single-photon avalanche diode with integrated quenching resistor [12] and 10 $\times$ 10 SiPM prototypes [13], [14]. In this paper we report the results of the first electrical and optical characterization performed on a 1 mm^2 total area SiPM fabricated in standard silicon planar technology at the STMicroelectronics Catania R&D clean room facility.

The measurements have been carried out by varying the temperature in order to study how the electrical and optical characteristics of the device change with this parameter.

We will show that the device performance is remarkable in terms of low dark noise rate and crosstalk probability, high photon detection efficiency and good linearity for weak photon fluxes. The results we have obtained on these first generation small area prototypes probably make our SiPM technology already suitable for their use in PET applications although other better performing large area samples are currently under production.

II. SIPM Description

A. Concept

The SiPM is a semiconductor photodiode operating in limited Geiger mode a few volts above its breakdown voltage. Its structure is based on a bidimensional pixel array of Geiger Mode Avalanche Photodiodes (GMAP) that individually act as photon counters. A photon counting diode cannot distinguish between multiple photons incident on the detector at the same time [15]. This limitation can be overcome by the SiPM. As it is schematically depicted in Fig. 1, in SiPM configuration each pixel is

Manuscript received December 10, 2008; revised April 03, 2009 and April 28, 2009. Current version published August 12, 2009.

M. Mazzillo, G. Condorelli, D. Sanfilippo, G. Valvo, B. Carbone, and G. Fallica are with Research and Development, IMS, STMicroelectronics, Catania 95121, Italy (e-mail: massimo.mazzillo@st.com).

S. Billotta, M. Belluso, and G. Bonanno are with INAF-Osservatorio Astrofisico di Catania, Catania 95123, Italy.

L. Cosentino, A. Pappalardo, and P. Finocchiaro are with INFN-Laboratori Nazionali del Sud, Catania 95125, Italy.

Color versions of one or more of the figures in this paper are available online at http://ieeexplore.ieee.org.

Digital Object Identifier 10.1109/TNS.2009.2024418

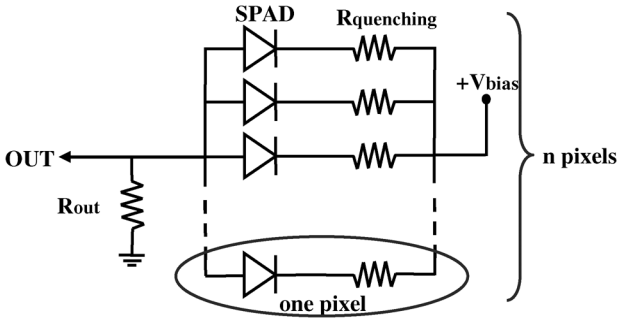

Fig. 1. Electrical scheme of the SiPM, its biasing circuit and output signal extraction. Each SPAD (Single Photon Avalanche Diode) in the array is connected to the power supply through an independent decoupling quenching resistor.

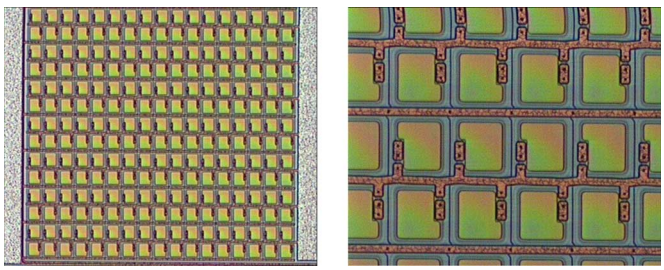

Fig. 2. Microphotograps of the 1 mm^2 SiPM prototype investigated in this work.

connected to the power supply through an integrated large series-quenching resistor which turns off the avalanche current and resets only the corresponding activated photodiode.

Since the outputs of the pixels are connected together, the amount of charge collected at the SiPM output is given by the analog superposition of the binary signals produced by all the activated pixels, which in turn is proportional to the number of incident photons (at the first order, when multiple hits on single cells can be neglected). Therefore the SiPM behaves like an analogue or proportional device for weak photon fluxes while its pixels work in a digital or Geiger mode [16].

B. SiPM Structure and Fabrication

The layout of the SiPM investigated in this work is presented in the microphotographs in Fig. 2. The device consists of 289 pixels and has a geometrical fill factor of 48%. Each microcell in the array has a square geometry with an active area $40 \times 40\ \mu\mathrm{m}^2$ and pitch 58 μm.

The SiPM structure is fabricated on silicon epitaxial p-type wafers and formed from planar $\mathrm{n}^+ - \mathrm{p}$ microcells. An implanted p-layer forms an enrichment region which defines the active area and breakdown voltage of the junction. The anode is contacted by p^+ sinkers created around the photodiode active area by means of a high-dose boron implantation. This structure serves to reduce the contact resistance of the anode, thereby providing a low resistance path for the avalanche current. The cathode is given by the diffusion of arsenic from a doped in-situ thin polysilicon layer deposited on the top of the structure. The n^+ layer overlaps the enrichment region to form a virtual guard ring in order to reduce the electric field at the edge of the diode and ensure a uniform breakdown region in the central area of each microcell. The quenching resistor, made from low-doped

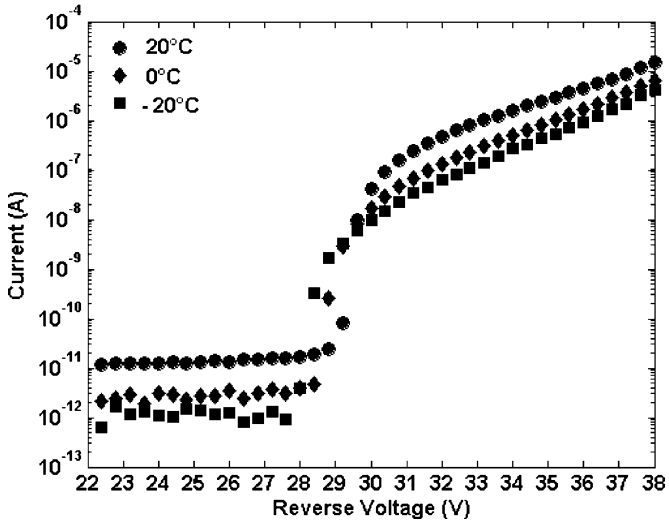

Fig. 3. Typical reverse I-V characteristics of a 1 mm^2 SiPM at different temperatures in the range $-20^\circ\mathrm{C} \div 20^\circ\mathrm{C}$.

polysilicon, is integrated on the cathode of the cell itself. Thin optical trenches filled with oxide and metal surround the pixel active area in order to reduce electro-optical coupling effects (crosstalk) between adjacent microcells. We also deposited a double-layer antireflective coating made of silicon oxide and silicon nitride and reduced the quasi-neutral region thickness above the thin junction depletion layer with respect to our previous GMAP technology [17], in order to enhance the spectral response of the device in the blue and near ultraviolet wavelength ranges.

III. Experimental Results

A. Static Characterization

On-wafer forward current, breakdown voltages (BV) and leakage current measurements were taken at room temperature on several 1 mm^2 SiPMs kept in dark condition using a temperature-controlled probe station and a semiconductor parameter analyzer (Agilent 4155C) [18]. In Fig. 3 we report the reverse characteristic at different temperatures in the range $-20^\circ\mathrm{C} \div 20^\circ\mathrm{C}$. At $20^\circ\mathrm{C}$ the BV is about 29.3 V and the leakage current is a few tens of picoamps. The low value of the leakage current indicates a low generation of electrical carriers both in the bulk as well as on the surface depleted region around the junction. Moreover, as expected, the higher the temperature the higher is the dark current above the breakdown voltage since the thermal generation from Shockley-Read-Hall (SRH) centers in the forbidden energy gap increases with the temperature [15].

As it has been already observed for single GMAPs with integrated quenching resistors [12], also for the 1 mm^2 SiPMs investigated in this work, the breakdown current is characterized by a parabolic growth for low overbias above the breakdown. This trend can be explained since the current flowing through the device above BV is given by the product of the dark noise rate of the device and the charge produced in the depletion layer in each avalanche event. Both these quantities depend linearly on the overvoltage (OV) applied to the device. In fact the

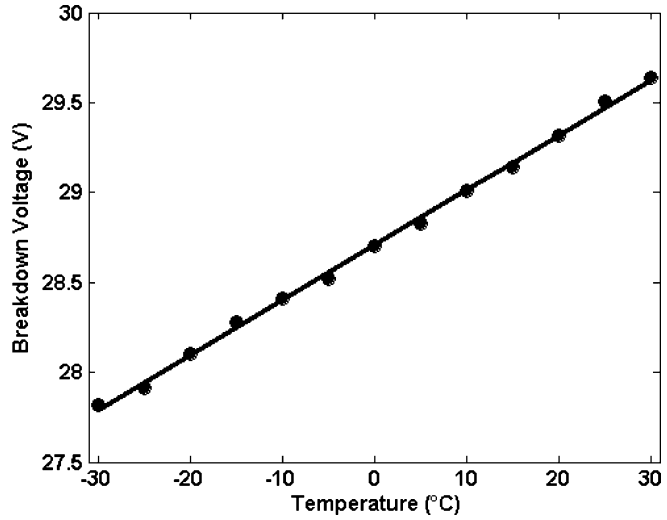

Fig. 4. SiPM breakdown voltage (BV) as a function of the temperature. BV increases linearly with a temperature coefficient of 30.6 $\mathrm{mV}/^{\circ}\mathrm{C}$.

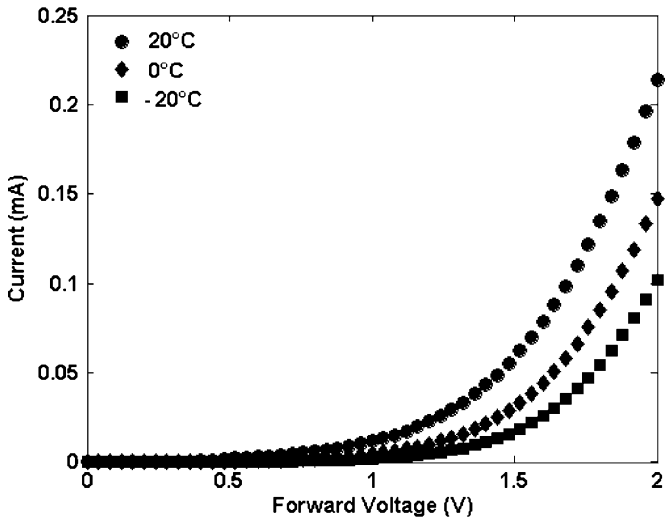

Fig. 5. Typical forward I-V characteristics of a 1 mm^2 SiPM at different temperatures in the range $-20^{\circ}\mathrm{C} \div 20^{\circ}\mathrm{C}$.

dark noise rate is proportional to the avalanche events triggering probability (Geiger efficiency), which in turn depends linearly on the overvoltage. At the same time the charge produced in each avalanche event is given by the product of the diode capacitance and the overbias applied to the device [5].

In Fig. 4 the behavior of the breakdown voltage value with the temperature is shown. BV linearly increases with T with a slope of 30.6 $\mathrm{mV}/^{\circ}\mathrm{C}$. This behavior is typical of a breakdown mechanism due to the avalanche multiplication produced by the impact ionization effect [19].

In Fig. 5 we report the forward characteristic obtained at different temperatures on a typical 1 mm^2 SiPM. The higher the temperature, the higher is the forward current flowing in the device. This means that the equivalent quenching resistor (i.e. the parallel of the quenching resistors of all the activated pixels), which limits the current flow in forward conditions, decreases at increasing temperature.

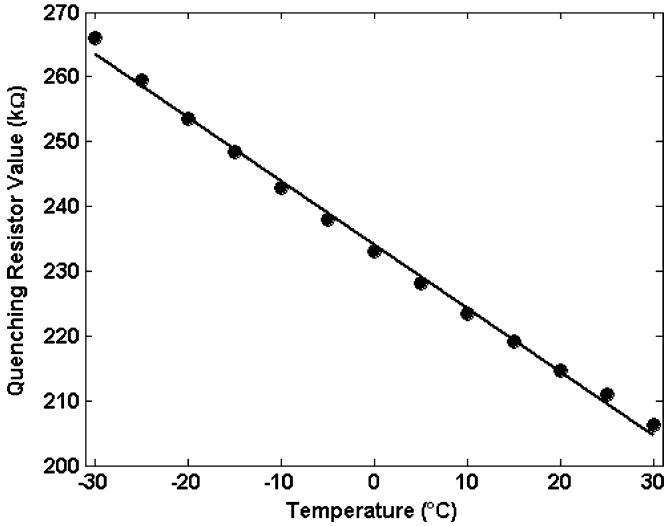

Fig. 6. Single cell quenching resistor value as a function of the temperature. The resistance value increases with decreasing temperature with a temperature coefficient of $-0.98\ \mathrm{k}\Omega/^{\circ}\mathrm{C}$.

The behavior of the individual quenching resistor value connected to each microcell with the temperature is shown in Fig. 6. The measurements were done on a single pixel identical to those contained within the SiPM array.

The resistance value is about 215 $\mathrm{k}\Omega$ at $20^{\circ}\mathrm{C}$ and linearly increases with decreasing temperature with a temperature coefficient of about $-0.98\ \mathrm{k}\Omega/^{\circ}\mathrm{C}$, due to the polysilicon conduction mechanism [20], [21].

All the measurements have been repeated on more than 500 devices, showing a very good uniformity (about 95%) of the breakdown voltages and resistance values and confirming the reliability of the polysilicon technology used for the quenching resistor fabrication.

B. Dynamic Characterization

1) Raw Signal: The operation of a SiPM biased a few volt above its breakdown voltage can be easily understood by observing the photodetector output pulses. Fig. 7 shows the Geiger pulses of a 1 mm^2 SiPM biased at 20%-OV as viewed on a 1 GHz bandwidth digital oscilloscope (Tektronix DPO 7104) [22], 50 Ω input impedance with an ac-coupled amplifier with a gain of 2.5. The device was kept at room temperature and in dark condition while the power supply Agilent E 3647A [18] was used for biasing the sensor.

The three Geiger pulses shown in the figure are the result of single pixels avalanching and the peak height of single pulses is usually referred to as the single photoelectron level. The pulse timing characteristics, as measured by the oscilloscope, are the results of the convolution of the microcells timing response and the readout electronics bandwidth. The rise time of Geiger pulses shown in the figure is about 1 ns while the quenching time is about 10 ns. The rise time is governed by the time the avalanche takes to spread all over the activated pixel active area while the quenching time is dominated by the product of the diode internal resistance (few $\mathrm{k}\Omega$) and the sum of parasitic and internal diode capacitances [12].

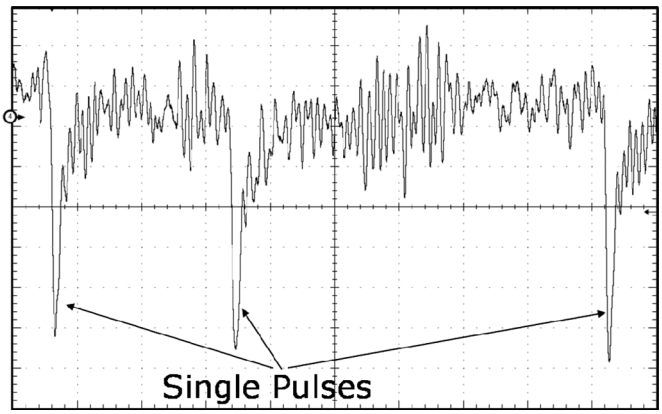

Fig. 7. Dark single pulses from a 1 mm^2 SiPM as viewed on an oscilloscope. The device was kept at room temperature and biased at 20%-Overvoltage. The units on x and y axis are 20 ns/div and 1 mV/div, respectively.

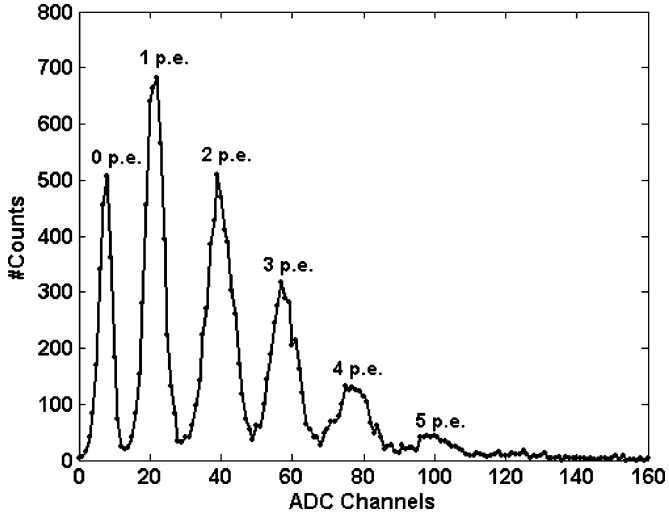

Fig. 8. Single photoelectron spectrum at room temperature from a 1 mm^2 SiPM. The spectrum was obtained at 31.8 V.

2) Gain: In a SiPM the gain is defined as the number of electron-hole pairs created in the depletion layer of the device during an avalanche event.

The gain was measured as a function of the overvoltage applied to the device by using the following standard NIM electronic modules:

- — TTL-NIM-ECL level adapters;
- — Lecroy 4608 leading edge discriminator;
- — Lecroy 222N gate and delay generator;
- — Lecroy 428F linear fan-in fan-out;
- — Lecroy 429A logic fan-in fan-out [23];
- — Fast amplifier, namely FTA810B, with gain 200 and rise time below 1 ns;
- — Cable delay units;
- — Silena 4418/Q CAMAC charge-to-digital converter;
- — Small multiparameter data acquisition system developed at Laboratori Nazionali del Sud-Catania.

An HP 6625A power supply [18] was used to bias the sensor while a 671-nm pulsed laser with fiber output and FWHM pulsewidth of 40 ps was used to illuminate the photodetector in a low light intensity condition [12], [14].

The SiPM was put into a light-tight box while the fiber coming from the laser was positioned just in front of it, making sure that the laser spot was covering the whole active area of the device. A nominal laser intensity of 2% was used for this measurement while the laser pulse repetition rate was fixed at 1 KHz. The gain measurement was done at room temperature. Following an approach similar to the one described in [14], the single photoelectron spectrum was obtained from the SiPM at each examined overvoltage value.

To obtain these spectra, the charge from the device was integrated for a fixed gate time of 40 ns. The integration window was set to coincide with the very fast optical pulse. In this way, the charge from 1 to n microcells, where n is the number peaks in the spectrum, was measured.

For each photoelectron peak a histogram, representing the distribution of the associated avalanche charge, was built; then each histogram was fitted with a gaussian function, whose centroid represents the average charge associated to the corresponding peak.

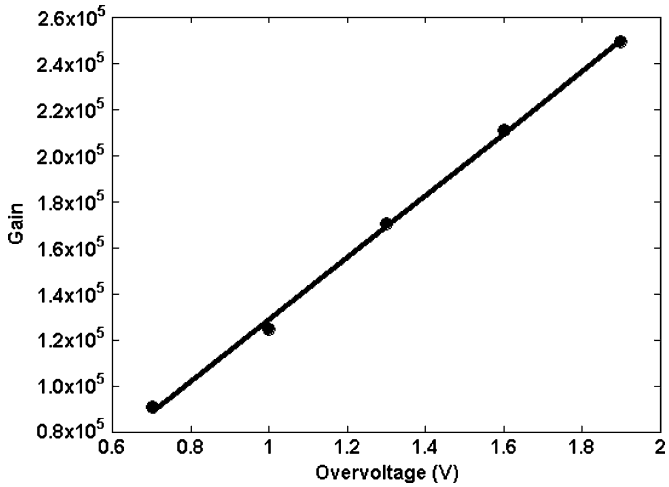

Fig. 9. Gain as a function of the overvoltage. The linear fit allows one to extrapolate the measured SiPM single cell capacitance which is about 20 fF.

The charge increment between adjacent peaks exactly equals the output charge of one detected photon. The gain can be easily obtained by dividing this quantity by the electron elementary charge [8], [14].

In Fig. 8 a typical single photoelectron spectrum obtained at 31.8 V is shown.

The first peak in the spectrum, called the pedestal, is a measure of the noise in the system (SiPM + electronics) and corresponds to cases when no avalanche events (Geiger pulses) were collected during the gate time. The second peak of the spectrum or the first photoelectron peak corresponds to a single pixel activated during the gate time. Subsequent peaks correspond to two, three and so on pixels firing during the gate time [8].

The spectra were acquired at five different overvoltage values and the gain corresponding to each OV is reported in Fig. 9.

The slope of the linear fit through the data points allows one to calculate the measured SiPM single cell capacitance which is of the order of 20 fF $(\Delta \mathrm{Q}/\Delta \mathrm{V})$ [4], [12], [14].

3) Dark Noise Rate: The main source of dark noise limiting the SiPM performances is the so-called primary dark count,

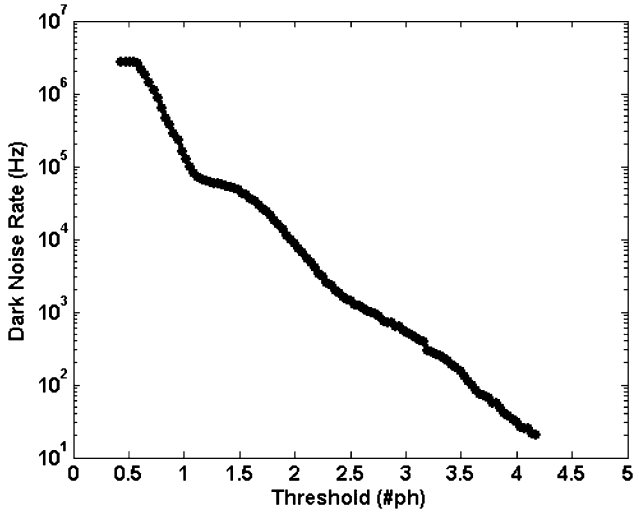

Fig. 10. Measured dark noise rate as a function of the discriminator threshold at 10%-OV bias. The threshold is normalized to the one-photon signal amplitude.

which mainly originates from carriers thermally generated through SRH centers in the depletion layer [15], [17].

Another important noise component in SiPM, due to the integration of many pixels on the same substrate, is represented by crosstalk effects. When a pixel is fired by the photon arrival, secondary photons, emitted by electroluminescence effect, can be absorbed in the active area of adjacent pixels in the SiPM array and trigger spurious avalanche events [17].

Finally the last source of spurious counts is represented by the afterpulsing. In fact during an avalanche event some carriers are trapped by deep levels in the multiplication region; released after a statistically fluctuating delay, they can re-trigger a Geiger event correlated with the previous avalanche pulse. Afterpulses depend on the trap concentration in the junction depletion layer as well as on the number of carriers generated during a Geiger pulse [17].

In order to measure the SiPM dark noise rate, the device was placed onto a thermally stabilized copper plate into a light-tight box. Then, by using the electronic setup already described in [13], the number of dark noise pulses generated per unit time was measured at different voltage bias as a function of the discriminator threshold (Lecroy 4608 leading edge discriminator [23]). A fast counter timer, namely Tennelec TC535P [24], was used to count the dark noise pulses.

The dark noise rate measured at 10%-OV and room temperature is reported in Fig. 10; in the plot the threshold is normalized to the one-photon signal amplitude.

The dark noise rate is about 2.7 MHz at the single photoelectron (1 p.e.) level (threshold at one half height of the 1 p.e peak) while it is reduced at 41 KHz at 2 p.e. (threshold at 1.5 p.e.).

An inter-pixel cross talk probability of 1.5% at 10%-OV can be estimated from the ratio of dark count rates at 2 p.e. and 1 p.e., after the correction for random coincidences [25], [26].

4) Photon Detection Efficiency (PDE): The Photon Detection Efficiency (PDE) in a SiPM is given by the product of three parameters: the quantum efficiency (QE), the avalanche triggering probability (ε), and the geometrical fill factor (η) [8].

$$PDE(\lambda, V) = QE(\lambda, V) \times \varepsilon(V) \times \eta. \tag{1}$$

The quantum efficiency QE is given by the product of the light transmission trough the dielectric layers on top of the silicon surface and the probability of photon absorption within the active area of the device. The triggering probability ε is the probability that an electron-hole pair triggers a self-sustaining avalanche in the depletion region. The geometrical fill factor η is the ratio of the active to total area of the microcell. A dead area around the microcell is due to the presence of the virtual guard ring and the structure preventing the optical cross-talk [8], [27].

The direct measurement of the SiPM PDE can be complicated by two effects; crosstalk and afterpulsing (see the Section III-B-3).

To eliminate the effect of crosstalk, the PDE has been determined by measuring the Quantum Detection Efficiency (QDE) of individual GMAPs identical to those contained within the SiPM array. The QDE is defined as the quantum efficiency of silicon QE times the carrier avalanche triggering probability ε. The SiPM PDE is then determined by scaling the QDE with the geometrical fill factor η. This method contains the afterpulsing in the microcell but eliminates the possible presence of crosstalk effects to the detected signal.

The experimental apparatus used to measure the QDE is schematically shown in Fig. 11.

We used a constant xenon lamp as luminous source, a system to select the wavelength of interest (a first module providing a series of neutral filters to tune the light intensity and a CZERNY-TURNER monochromator) and a beam splitter to direct the monochromatic radiation towards an integrating sphere hosting a calibrated reference photodiode and the GMAP. The sphere was used to obtain a uniform illumination on both detectors, while the reference photodiode, traced by the National Institute of Standard and Technology (NIST), served to measure the flux of the incident radiation on the GMAP [25].

The GMAP was biased with a constant voltage a few volt above its breakdown voltage. Since the GMAP works as a binary device, as long as there are no charge carriers inside its active area, no current flows in the photodiode. When an electrical carrier, thermally or photogenerated, is injected in the depletion layer, a sharp current pulse in the milliampere range and with subnanosecond rise time is produced due to the self-sustaining avalanche multiplication process [15]. An active quenching circuit (AQC) connected to the GMAP was used to sense the leading edge of the avalanche current, to turn off the device for a suitable hold-off time and finally to restore the voltage to the bias value [28]. For our measurements we used a hold-off time of 20 μs in order to minimize the contribution of afterpulsing events to the measured signal. During the hold-off time the device is kept below the breakdown voltage; therefore carriers released during this time window can not trigger an avalanche event [17].

The AQC output was connected to a USB digital counter in order to acquire the counts on the PC. We simultaneously

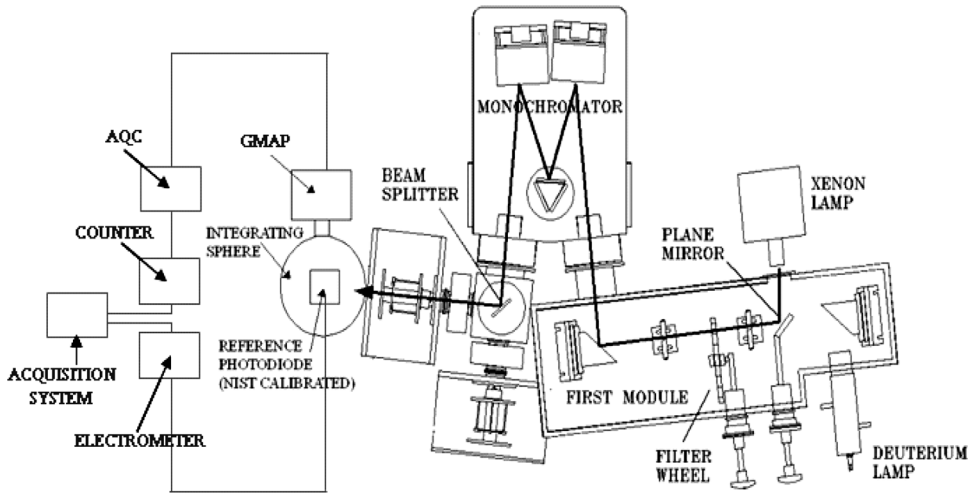

Fig. 11. Experimental set-up used for QDE measurements.

measured the signal from the reference photodiode through a Keithley 6514 electrometer [29] connected through an IEEE 488 parallel interface. An automated procedure was used to calculate the GMAP QDE during the measurements. Counting losses, due to the probability that a photon is absorbed in the pixel active area during the hold-off time, have been taken into account by using a classical dead time correction formula:

$$R_{Est} = \frac{R_{Meas}}{1 - T_{Hold-off} R_{Meas}} \tag{2}$$

where $\mathrm{R_{Meas}}$ is the measured counting rate and $\mathrm{R_{Est}}$ is the estimated counting rate, corrected from the losses due to the hold-off time $\mathrm{T_{Hold-off}}$ [29].

The measurements were done at different overvoltage by placing the device in a climatic chamber to control the detector temperature. The incident flux over the GMAP active area was less than 1×10^6 photons/s in all the investigated wavelength range; the corresponding measured counting rates were in the range 5×10^3 s^{-1} $-$ 1×10^5 s^{-1} according to the different single cell response to the light wavelength and the applied overvoltage.

Fig. 12 shows the QDE measured on a typical single cell scaled for the geometrical efficiency of the SiPM array (48%) as a function of the photon wavelength and the applied overvoltage.

The measurements shown in the figure were done at the fixed temperature of 20°C. The device exhibits a remarkable PDE in the wavelength range 400–500 nm with a maximum at around 500 nm. Peak detection efficiency at 20%-OV (about 20%) is a very good result with respect to the quantum detection efficiency measured on our previous GMAP technology [17]. Moreover, as expected, the PDE increases with the overvoltage since the avalanche triggering probability increases with the overbias.

The same measurements were performed by varying the temperature applied to the device. In Fig. 13 we report the PDE results obtained at the fixed 10%-OV and at three different temperatures ($-$20°C, 0°C and 20°C). To calculate the overvoltage at each temperature, we have taken in account the variation of

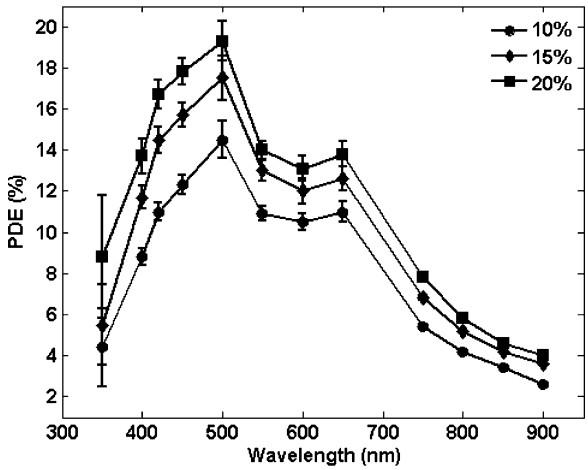

Fig. 12. SiPM Photon Detection Efficiency (PDE) at 20°C and increasing overvoltage.

the breakdown voltage with T, according to the characterization shown in Fig. 4. From the figure it can be seen that the PDE slightly increases at lower temperature in the near ultraviolet and visible wavelength ranges.

To further investigate this phenomenon, we measured the PDE at the fixed wavelength of 420 nm by varying the temperature and the overvoltage applied to the device. We have chosen this particular wavelength in view of the design and manufacturing of large area SiPM to be used as photodetectors in Positron Emission Tomography (PET). In fact in this application the SiPM is usually coupled to Lutetium Orthosilicate (LSO) or Lutetium-Yttrium Orthosilicate (LYSO) scintillators which have a peak emission wavelength just at 420 nm [27], [31].

As shown in Fig. 14, the PDE decreases with increasing T with a temperature coefficient of about $-0.3\%/°\mathrm{C}$. This result seems to be not dependent on the overvoltage applied to device. This behavior could be ascribed to the increase of the avalanche triggering probability with decreasing temperature [32]. In the near-infrared this effect could be hidden by the limited SiPM

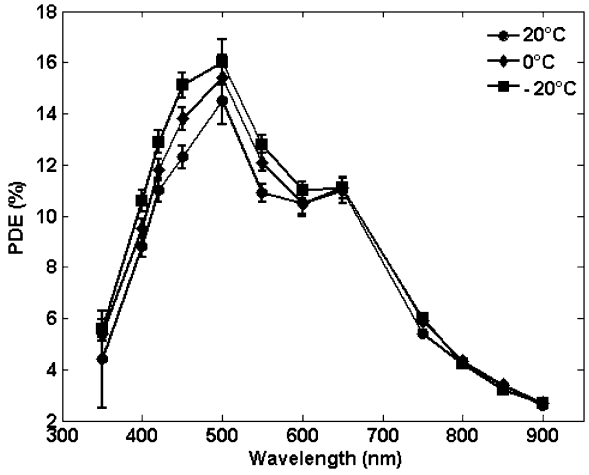

Fig. 13. SiPM PDE at 10%-OV and increasing temperature.

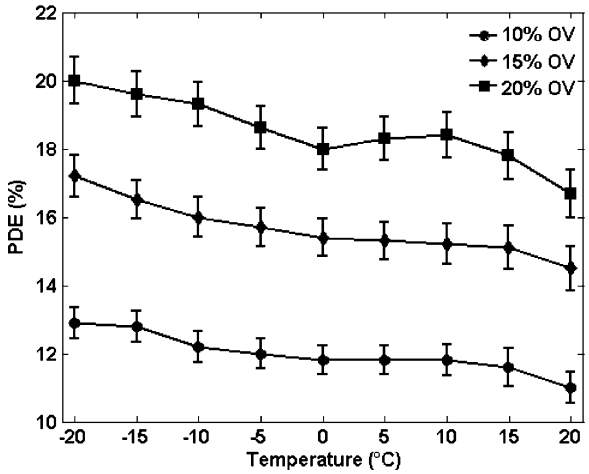

Fig. 14. SiPM PDE at 420 nm at increasing temperature and overvoltage.

signal to noise ratio due to the weak incident photon flux and poor detector sensitivity in this wavelength range.

5) Linearity and Dynamic Range: Since the SiPM has a finite number of pixels, the dynamic range (i.e. the maximal number of photons that can be simultaneously detected) is limited. The SiPM PDE and the total number of microcells determine the photodetector dynamic range. A larger pixel size leads generally to a higher fill factor, and therefore to a higher PDE. However, for a fixed SiPM size, increasing the microcell size also results in a reduction of the number of pixels and consequently of the dynamic range of the device [8].

The most appropriate measurement to test SiPM linearity is to illuminate the photodetector with extremely short laser pulses and measure the signal charge at different light photon fluxes. However the experimental setup used for the optical measurements and described in the previous paragraph is not equipped with a laser. Therefore to perform the linearity tests on our devices, the photocurrent at the SiPM output was measured as a function of the photon rate incident upon the detector area. In this type of measurement also the recharging time contribute to the determination of the SiPM dynamic range. In fact the higher

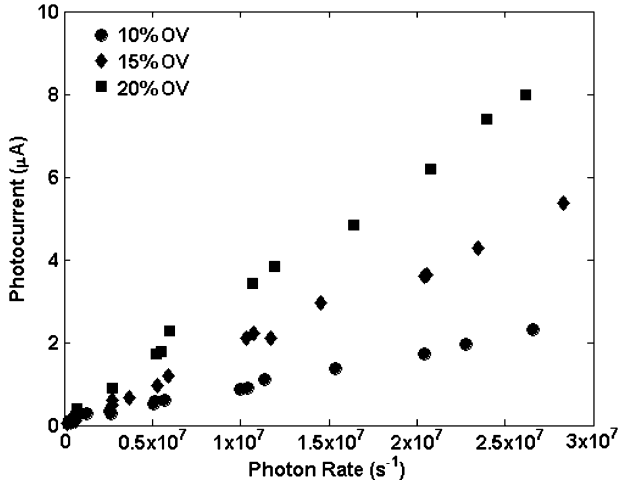

Fig. 15. SiPM photocurrent as a function of the incident photon rate at 450 nm. The measurements were done at increasing OV at the fixed temperature of 20°C.

the quenching resistor value and consequently the recharging time [28], the lower the dynamic range.

The linearity measurements were done by using a series of neutral filters and varying the monochromator exit slit width to tune the light intensity in the experimental apparatus shown in the Section III-B-4. A maximum incident photon rate of about 3×10^7 ph/s was obtained on the 1 mm^2 SiPM area by increasing as much as possible the monochromator exit slit width (5 mm) and without using any neutral filters.

The SiPM dark current was first measured at all the overvoltage and temperature values used for the characterization and then subtracted from the current of the device measured when it was exposed to the luminous flux. A Keithley 6514 electrometer [29] was used to measure the SiPM current.

Fig. 15 shows the photocurrent measured at the output of a typical 1 mm^2 SiPM as a function of the photon rate incident on the device and the applied overvoltage. These measurements were done at 450 nm at the fixed temperature of 20°C.

The SiPM response at the three examined overbias is perfectly linear in all the investigated incident photon rate range.

The SiPM linearity was also tested as a function of the photons wavelength. In Fig. 16 we report the SiPM photocurrent measured at 450 nm, 550 nm and 750 nm wavelengths. These measurements were done at 20%-OV at the fixed temperature of 20°C.

The photocurrent values at 550 nm and 750 nm do not saturate in the investigated photon rate range as it also happens at 450 nm. This result was somewhat expected since the PDE measured at 550 nm and 750 nm is lower than the PDE at 450 nm (see Fig. 12) and the lower the PDE, the lower the number of activated pixels.

To test the behavior of the linearity with the temperature, the same measurements were done by varying the temperature applied to the photodetector. In Fig. 17 we report the SiPM photocurrent at 450 nm and at 20%-OV at three different temperatures (−20°C, 0°C and 20°C).

The lower the temperature, the higher the photocurrent since the PDE increases with decreasing temperature (see Fig. 13).

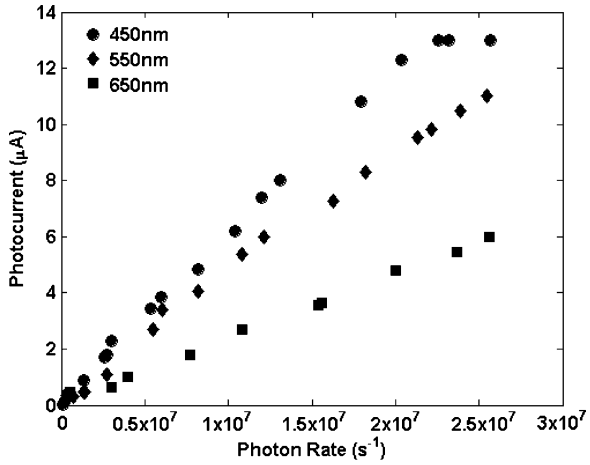

Fig. 16. SiPM photocurrent as a function of the incident photon rate at 450 nm, 550 nm and 750 nm. The measurements were done at 20%-OV at the fixed temperature of 20°C.

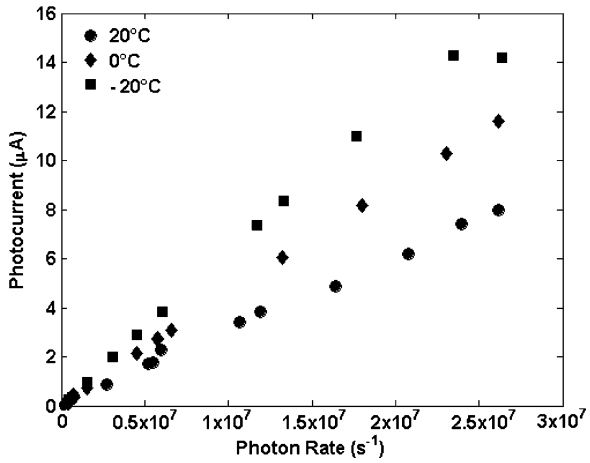

Fig. 17. SiPM photocurrent as a function of the incident photon rate at 450 nm. The measurements were done at 20%-OV at increasing temperatures.

However notwithstanding the increase of the current, the device shows a good linearity up to about 2.5×10^7 ph/s also at $-20°\mathrm{C}$ and $0°\mathrm{C}$.

The measurement results shown in this paragraph probe the good linearity of the photodetector response in the low light level region of the SiPM detection capability. In the near future we will modify the optical setup to test the detector dynamic range using higher light photon rates and reproduce the photodetector illumination condition in PET applications.

In this case, for instance, for 511 keV gamma-ray photons and LSO or LYSO scintillators, one will be expecting about 4000–6000 photons reaching the SiPM microcells within 40–80 ns [31]. In this situation the light photon rate incident on the SiPM area is several orders of magnitude higher than 3×10^7 ph/s achievable as maximum photon rate with the present optical setup.

IV. Conclusions and Outlook

In this paper, a thorough electrical and optical characterization of the first 1 mm^2 SiPM prototypes fabricated at the STMicroelectronics Catania R&D facility, has been reported. The optical characterization has been performed as a function of the temperature applied to the SiPM.

The main features of this device are: breakdown voltage of 29.3 V at room temperature; gain of the order of 10^5 growing linearly with the overvoltage; dark noise rate of 2.7 MHz (threshold at 0.5 p.e) and inter-pixel crosstalk probability of 1.5% measured at 10%-OV and room temperature, PDE of about 14% measured at 500 nm, 10%-OV and 20°C, good linearity up to about 3×10^7 ph/s measured at 450 nm, 10%-OV and 20°C. The tests have been performed on several samples showing very uniform characteristics. By comparing the results shown in this paper with the measurement values reported on SiPMs with the same total area and tested in similar operating conditions, we find that the electrical and optical performances of our devices are comparable to or better than those described in [3], [5], [7]–[9].

In the immediate future, the 1 mm^2 SiPMs investigated in this paper will be coupled with LSO scintillators and irradiated with gamma-ray photons of different energies for energy resolution, coincidence timing resolution and linearity measurements.

However the results we have obtained so far on these first generation small area prototypes and shown in this paper can be considered really promising for the forthcoming production of large-area SiPM to be used as photodetectors in PET applications.

References

[1] D. Renker, "Geiger-mode avalanche photodiodes, history, properties and problems," *Nucl. Instrum. Methods Phys. Res. A*, vol. A567, pp. 48–56, 2006.

[2] I. Britvitch, E. Lorenz, A. Olshevski, D. Renker, Z. Sadygov, R. Scheuermann, A. Stoykov, A. Werner, and I. Zheleznykh, "Development of scintillation detectors based on avalanche microchannel photodiodes," *Nucl. Instrum. Methods Phys. Res. A*, vol. A571, pp. 317–320, 2007.

[3] V. Golovin and V. Saveliev, "Novel type of avalanche detector with Geiger mode operation," *Nucl. Instrum. Methods Phys. Res. A*, vol. A518, pp. 560–564, 2004.

[4] P. Buzhan, B. Dolgoshein, L. Filatov, A. Ilyin, V. Kaplin, A. Karakash, S. Klemin, R. Mirzoyan, A. N. Otte, E. Popova, V. Sosnovtsev, and M. Teshima, "Large area silicon photomultipliers: Performance and applications," *Nucl. Instrum. Methods Phys. Res. A*, vol. A567, pp. 78–82, 2006.

[5] C. Piemonte, R. Battiston, M. Boscardin, G. Dalla Betta, A. Del Guerra, N. Dinu, A. Pozza, and N. Zorzi, "Characterization of the first prototypes of silicon Photomultiplier Fabricated at ITC-irst," *IEEE Trans. Nucl Sci.*, vol. 54, no. 1, pp. 236–244, Feb. 2007.

[6] C. J. Stapels, F. L. Augustine, M. R. Squillante, and J. F. Christian, "Characterization of CMOS solid-state photomultiplier for a digital radiation rate meter," in *Proc. IEEE Nuclear Science Symp. Conf. Rec.*, 2006, vol. 2, pp. 918–922.

[7] K. Yamamoto, K. Yamamura, K. Sato, S. Kamakura, T. Ota, H. Suzuki, and S. Ohsuka, "Development of Multi-Pixel Photon Counter (MPPC)," in *Proc. IEEE Nuclear Science Symp. Conf. Rec.*, 2006, vol. 2, pp. 1094–1097.

[8] A. G. Stewart, V. Saveliev, S. J. Bellis, D. J. Herbert, P. J. Hughes, and J. C. Jackson, "Performance of 1- mm^2 silicon photomultiplier," *IEEE J. Quantum Electron.*, vol. 44, no. 2, pp. 157–163, 2008.

[9] B. Dolgoshein, V. Balagura, and P. Buzhan *et al.*, "Status report on silicon photomultiplier development and its applications," *Nucl. Instrum. Methods Phys. Res. A*, vol. A563, pp. 368–376, 2006.

[10] E. Grigoriev, A. Akindinov, M. Breitenmoser, S. Buono, E. Charbon, C. Niclass, I. Desforges, and R. Rocca, "Silicon photomultipliers and their bio-medical applications," *Nucl. Instrum. Methods Phys. Res. A*, vol. A571, pp. 530–533, 2007.

[11] N. Otte, B. Dolgoshein, J. Hose, S. Klemin, E. Lorenz, R. Mirzoyan, E. Popova, and M. Teshima, "The potential of SiPM as photon detector in astroparticle physics experiments like MAGIC and EUSO," *Nucl. Phys. B (Proc. Suppl.)*, vol. 150, pp. 144–149, 2006.

[12] M. Mazzillo, G. Condorelli, A. Piazza, D. Sanfilippo, G. Valvo, B. Carbone, G. Fallica, S. Billotta, M. Belluso, G. Bonanno, A. Pappalardo, L. Cosentino, and P. Finocchiaro, "Single-photon avalanche photodiodes with integrated quenching resistor," *Nucl. Instrum. Methods Phys. Res. A*, vol. A591, pp. 367–373, 2008.

[13] P. Finocchiaro, A. Pappalardo, L. Cosentino, M. Belluso, S. Billotta, G. Bonanno, B. Carbone, G. Condorelli, S. Di Mauro, G. Fallica, M. Mazzillo, A. Piazza, D. Sanfilippo, and G. Valvo, "Characterization of a novel 100-channel silicon photomultiplier—Part I: Noise," *IEEE Trans. Electron Devices*, vol. 55, no. 10, pp. 2757–2764, 2008.

[14] P. Finocchiaro, A. Pappalardo, L. Cosentino, M. Belluso, S. Billotta, G. Bonanno, B. Carbone, G. Condorelli, S. Di Mauro, G. Fallica, M. Mazzillo, A. Piazza, D. Sanfilippo, and G. Valvo, "Characterization of a novel 100-channel silicon photomultiplier—Part II: Charge and time," *IEEE Trans. Electron Devices*, vol. 55, no. 10, pp. 2765–2773, 2008.

[15] M. Ghioni, A. Gulinatti, I. Rech, F. Zappa, and S. Cova, "Progress in silicon single-photon avalanche diodes," *IEEE J. Sel. Topics Quantum Electron.*, vol. 13, no. 4, pp. 852–862, 2007.

[16] P. Buzhan, B. Dolgoshein, A. Ilyin, V. Kantserov, V. Kaplin, A. Karakash, A. Pleshko, E. Popova, S. Smirnov, Y. Volkov, L. Filatov, S. Klemin, and F. Kayumov, "An advanced study of silicon photomultiplier," *ICFA Instrum. Bull.*, vol. 23, pp. 28–41, 2001.

[17] M. Mazzillo, G. Condorelli, and A. Campisi *et al.*, "Single photon avalanche photodiodes arrays," *Sens. Actuators A*, vol. 138, pp. 306–312, 2007.

[18] [Online]. Available: http://www.agilent.com

[19] M. Petasecca, B. Alpat, G. Ambrosi, P. Azzarello, R. Battiston, M. Ionica, A. Papi, G. U. Pignatel, and S. Haino, "Thermal and electrical characterization of silicon photomultiplier," *IEEE Trans. Nucl Sci.*, vol. 55, no. 3, pp. 1686–1690, Jun. 2008.

[20] C. Piemonte, M. Boscardin, G.-F. Dalla Betta, M. Melchiorri, N. Zorzi, R. Battiston, A. Del Guerra, and G. Llosa, "Recent developments on silicon photomultipliers produced at FBK-irst," in *Proc. IEEE Nuclear Science Symp. Conf. Rec.*, 2007, vol. 3, pp. 2089–2092.

[21] H. Otono, S. Yamashita, T. Yoshioka, H. Oide, H. Hano, and T. Suehiro, "Study of MPPC at liquid nitrogen temperatures," in *Proc. Int. Workshop New Photon Detectors PD07*, Kobe, Japan, Jun. 27–29, 2007, Kobe Univ..

[22] [Online]. Available: http://www.tektronix.com

[23] [Online]. Available: http://www.lecroy.com

[24] [Online]. Available: http://www.canberra.com

[25] S. Uozumi, "Study and development of multi pixel photon counter for the GLD calorimeter readout," in *Proc. Int. Workshop New Photon-Detectors PD07*, Kobe, Japan, Jun. 27–29, 2007, Kobe Univ..

[26] P. S. Marrocchesi, M. G. Bagliesi, K. Batkov, G. Bigongiari, M. Y. Kim, T. Lomtadze, P. Maestro, F. Morsani, and R. Zei, "Active control gain of a 3 mm × 3 mm silicon photomultiplier," *Nucl. Instrum. Methods Phys. Res. A*, vol. A602, pp. 391–395, 2009.

[27] M. Mazzillo, A. Piazza, G. Condorelli, D. Sanfilippo, G. Fallica, S. Billotta, M. Belluso, G. Bonanno, L. Cosentino, A. Pappalardo, and P. Finocchiaro, "Quantum detection efficiency in Geiger mode avalanche photodiodes," *IEEE Trans. Nucl. Sci.*, vol. 55, no. 6, pp. 3620–3625, Dec. 2008.

[28] S. Cova, M. Ghioni, A. Lacaita, C. Samori, and F. Zappa, "Avalanche photodiodes and quenching circuits for single-photon detection," *Appl. Opt.*, vol. 35, no. 12, pp. 1956–1976, 1996.

[29] [Online]. Available: http://www.keythley.com

[30] E. Sciacca, E. A. C. Giudice, and D. Sanfilippo *et al.*, "Silicon planar technology for single-photon optical detectors," *IEEE Trans. Electron Devices*, vol. 50, no. 4, pp. 918–925, 2003.

[31] C. L. Melcher and J. S. Schweitzer, "Cerium-doped lutetium oxyorthosilicate: A fast efficient new scintillator," *IEEE Trans. Nucl Sci.*, vol. 39, no. 4, pp. 502–505, Aug. 1992.

[32] I. Rech, I. Labanca, G. Armellini, A. Gulinatti, M. Ghioni, and S. Cova, "Operation of silicon single photon avalanche diodes at cryogenic temperature," *Rev. Sci. Instrum.*, vol. 78, no. 6, pp. 063105–063107, 2007.